Article

Rheology of Poly(α-olefin) Bottlebrushes: Effect of Self-Dilution by Alkane Side Chains

Manfred H. Wagner* and Valerian Hirschberg*

Read Online

ACCESS | Metrics & More | Article Recommendations

ABSTRACT: Bottlebrush polymers are combs with extremely high grafting density along their backbone chain. We consider the rheology of bottlebrush poly(α-olefins) with side chains ranging from 6 carbons [poly(1-octene)] to 16 carbons [poly(1-octadecene)] as investigated by López-Barrón et al. (J. Rheol. **2019**, *63* (6), 917−926). We argue that the backbone chain of poly(α-olefins) is diluted by the unentangled alkane side chains and that the rheology of poly(α-olefin) bottlebrushes is equivalent to that of poly(1-methylethylene), i.e., atactic polypropylene diluted by a low-molecular-weight solvent. We show that this approach is in agreement with the decreasing plateau modulus of the poly(α-olefins) with increasing side chain length, and it allows to replace empirical correlations by a relation based on physical arguments. The specific strong transient strain hardening in elongational flow shows similar features as observed for entangled solutions of linear polymers and can be explained by the enhanced relaxation of stretch model if self-dilution of the poly(α-olefins) is taken into account. Due to the large difference between the disengagement time τ_d and Rouse time τ_R, the orientation and stretch of backbone chains are well separated, and strain hardening starts after full orientation at Weissenberg numbers above $Wi_R = \dot{\varepsilon}\tau_R \cong 0.3$. The amount of strain hardening increases with increasing dilution, and at high Wi_R, all poly(α-olefins) are expected to reach the same steady-state elongational stress.
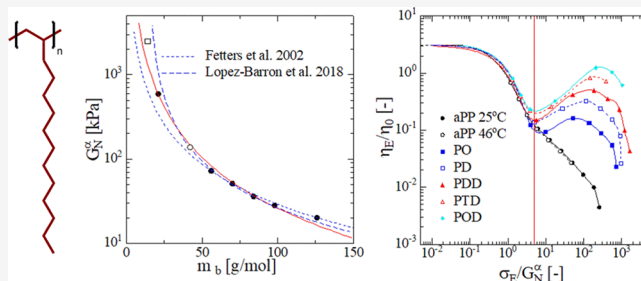
1. INTRODUCTION

As summarized in a recent review,[4] comb and bottlebrush polymers show a rich variety of rheological and mechanical properties that can be controlled through their molecular characteristics, such as the backbone and side chain lengths as well as the number of branches per molecule or the grafting density. Of particular interest to industrial applications like film blowing, fiber spinning, and foaming is the amount of strain hardening in elongational flow.[5] In order to induce substantial strain hardening, at least two branch points with long-chain branching (LCB) per molecule are needed as shown by McLeish and Larson.[6] The side chains length has to be above the entanglement molecular weight M_e in order to pin segments of the backbone between two branch points to the deforming matrix and postpone stretch relaxation until the side chains are withdrawn into the tube of the backbone. Abbasi and co-workers[7] investigated the impact of the number of LCB branches from loosely crafted combs to bottlebrushes and observed that the strain hardening factor increases significantly with increasing number of branches. Transient strain hardening is defined as the relative upward deviation of the elongational stress growth coefficient from the linear viscoelastic envelope. The term "bottlebrush" refers to polymer topologies with the coil size of the side chains being equal to or greater than the

spacing between branch points along the backbone. If the side chains are shorter and have molecular weights below M_e, they can no longer restrict stretch relaxation of backbone segments, and there should be no strain hardening at strain rates below the inverse of the Rouse time. However, recently López-Barrón et al.[2,3] reported that bottlebrush polymers can exhibit substantial strain hardening even under circumstances where no backbone segments pinned by side chains exist. They investigated the elongational rheology of high molecular weight poly(α-olefin) bottlebrushes ranging from poly(1-octene) to poly(1-octadecene) prepared by the polymerization of 1-alkene monomers. From a molecular point of view, these are the simplest bottlebrush polymers as both the backbone and the side chains consist of linear alkanes. The lower plateau moduli of the poly(α-olefins) were explained by steric repulsion between the side chains, with longer side chains leading to larger persistence lengths and resulting in higher entanglement molecular weights
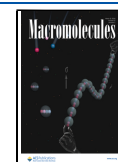
Table 1. Molecular Characterization of Bottlebrush

polymer	M_w[kg/mol]	M_w/M_n [-]	M_e[kg/mol]	G_N^α [kPa]	Z [-]	T_g [°C]	T_m [°C]	ρ [kg/m³]
poly(1-methylethylene), aPP	233	1.82	3.88	590	60			864
poly(1-octene), PO	3030	2.41	27.1	72.5	112	−63.5		792
poly(1-decene), PD	3160	2.43	38.0	51.1	83.2	−68.0	−0.65	784
poly(1-dodecene), PDD	3960	2.48	55.3	35.9	71.6	−66.5	25.9	801
poly(1-tetradecene), PTD	4820	2.12	74.2	28.2	65.0		43.1	803
poly(1-octadecene), POD	5870	2.50	109	20.1	53.9		54.1	762

M_e. López-Barrón and co-workers[2,3] observed substantial transient strain hardening of the elongational stress growth coefficient of the poly(α-olefins) investigated and attributed this to an increase in side chain interdigitation as soon as the polymers align in the flow direction. This was postulated to increase intermolecular friction, leading to enhanced transient strain hardening. However, to date, no constitutive model has been advanced to predict the elongational rheology of these bottlebrush polymers with entangled backbone and unentangled side chains and explain quantitatively why they are capable of strain hardening.

According to a recent review by Matsumiya and Watanabe,[8] the change of monomeric friction with segmental orientation is the key in understanding the elongational rheology of linear polymer melts and concentrated polymer solutions. While the universality of the linear viscoelastic behavior of well-entangled monodisperse linear polymer melts and solutions is well established based on only three material parameters (plateau modulus, characteristic time, and number of entanglements), this universality is lost in the nonlinear viscoelastic regime as especially apparent in elongational flow, where differences in the rheology of melts and solutions become apparent. While the elongational viscosity of linear polymer melts shows monotonous strain-rate thinning, solutions show strain-rate thinning, followed by strain-rate hardening, see, e.g., ref 9. According to Ianniruberto et al.,[31,32] strain-rate thinning is caused by the reduction of segmental friction of highly oriented/stretched polymer chains in linear melts under fast extensional flows. The magnitude of this friction reduction diminishes with decreasing polymer concentration in solution, resulting in the nonuniversality of the elongational rheology of polymer melts and solutions. However, so far the effect of friction reduction has been modeled by the use of empirical functions related to segmental orientation or elongational stress with parameters fitted to experimental data of elongational viscosities. A perspective on recent findings in extensional rheology for polymer melts and solutions with different macromolecular architectures was presented by Huang.[33]

In the context of tube models with varying tube diameter, Wagner and Narimissa[10] proposed the enhanced relaxation of stretch (ERS) model and showed that the stretch evolution equation of the ERS model can be expressed in terms of monomeric friction reduction. Instead of empirical correlations between friction coefficient and segmental orientation, the ERS model provides an analytical and parameter-free relation of friction reduction as a function of chain stretch. By primitive chain network simulations using the parameter-free universal relation of monomeric friction reduction derived from the ERS model, Wagner et al.[11] demonstrated the equivalence with empirical friction reduction models for three poly(propylene carbonate) melts and a polystyrene (PS) melt.

The objective of this contribution is to show that the elongational rheology of the poly(α-olefin) bottlebrushes

investigated by López-Barrón and co-workers[2] can be explained by the ERS model, if dilution of the backbone by the side chains is taken into account. We first summarize the molecular and linear viscoelastic characterization of the poly(α-olefins) and show that the decreasing plateau modulus with increasing side chain length is a consequence of self-dilution of the backbone by the alkane side chains. We then give a short summary of the ERS model, followed by a comparison of experimental data and model predictions. The modeling is based exclusively on the molecular and linear viscoelastic characterization of the poly(α-olefins) and without the use of any free parameter.

2. MOLECULAR AND LINEAR VISCOELASTIC CHARACTERIZATION OF POLY(α-OLEFIN) BOTTLEBRUSHES

The molecular properties of the bottlebrush poly(α-olefins) with side chains from 6 carbons (poly(1-octene)) to 16 carbons (poly(1-octadecene)) are taken from López-Barrón et al.[1−3] They also considered an atactic poly(1-methylethylene), i.e., atactic polypropylene (aPP) at two temperatures to compare the rheological response of the bottlebrush polymers with that of a linear polyolefin. The entanglement molecular weight was calculated by

$$M_e = \frac{\rho R T}{G_N^\alpha} \tag{1}$$

ρ is the density measured at 25 °C for aPP, PO, PD, and PDD and at 70 °C for PTD and POD, R the gas constant, T the absolute temperature, and G_N^α the plateau modulus of the poly(α-olefins). In addition, Table 1 summarizes the number $Z = M_w/M_e$ of entanglements, the glass transition temperature T_g, and the melting temperature T_m (measured as the second (high temperature) peak in the DSC traces[1]). All bottlebrush polymers have well-entangled backbones.

From the mastercurves of G' and G'', parsimonious relaxation spectra were obtained

$$G(t) = \sum_i g_i \exp(t/\tau_i) \tag{2}$$

for characterization of the linear viscoelasticity all polymer systems considered here. The partial moduli g_i and relaxation times τ_i as determined by the IRIS software[9,10] resulted in excellent agreement with the linear viscoelastic data of G' and G'', see Figure 1 and the Support Information.[2] We calculated the zero-shear viscosity η_0 and the mean quadratic average of the relaxation times taken as disengagement time τ_d from the discrete relaxation spectra:

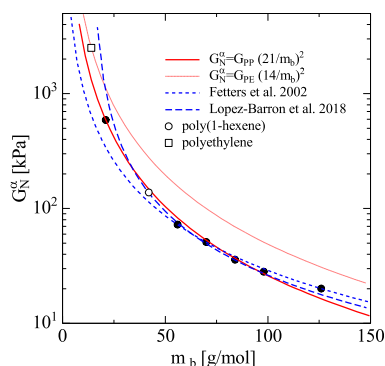$$\eta_0 = \sum_i g_i \tau_i \tag{3}$$

and

Figure 1. Plateau modulus G_N^α as a function of the molecular weight m_b per backbone bond of α-olefins. Data (symbols) from Lopéz-Barrón and co-workers[1] and Fetters et al.[13]

$$\tau_d = \frac{\sum_i g_i \tau_i^2}{\sum_i g_i \tau_i} \tag{4}$$

We use Osaki's approach[12] for the quantification of the Rouse stretch relaxation time τ_R, which extrapolates the Rouse time of unentangled polymer systems to the Rouse time of the melt and takes into account the power of 3.4 scaling of the zero-shear viscosity with molecular weight M

$$\tau_R = \frac{12 M \eta_0}{\pi^2 \rho R T}\left(\frac{M_c}{M}\right)^{2.4} \tag{5}$$

As the bottlebrush melts considered are polydisperse with polydispersities M_w/M_n of 1.8−2.5 and the Rouse time will be dominated rather by the longer polymer chains, we identify M here with the z-average M_z of the molecular weight and assume a log-normal molecular weight distribution, i.e.,

$$M \cong M_z \approx M_w^2/M_n \tag{6}$$

The critical molecular weight M_c, which is the molecular weight when the entanglement effect becomes apparent by a change of the power-law exponent of the zero-shear viscosity scaling from 1 to 3.4, is typically related to M_e by a factor of 2 to 3. We take the relation

$$M_c = 2.5 M_e \tag{7}$$

in the following. As seen from Table 2, τ_R and τ_d are separated by 2−3 orders of magnitude. Due to the different molecular weights and the different measurement temperatures T, τ_R and τ_d of the poly(α-olefins) cannot be compared directly between the samples.

As seen in Table 1, the plateau modulus G_N^α of the bottlebrush poly(α-olefins) decreases with increasing number N_{sc} of side chain bonds or increasing molecular weight m_b per backbone

bond. Fetters et al.[13] reported the following empirical correlation for poly(α-olefins),

$$G_N^\alpha = 41.84 m_b^{-1.58} \tag{8}$$

with the prefactor in units of MPa and based on the range of 35 g/mol $\leq m_b \leq$ 56 g/mol. Fetters and co-workers noted that this relation is strictly empirical, and there is no justification for this correlation, except that it fits the data. Lopéz-Barrón and co-workers[1] expressed the dependence of G_N^α on N_{sc} by a power law decay function of the form

$$G_N^\alpha = 1.05 N_{sc}^{-1.47} \equiv 1.05\left(\frac{m_b}{7} - 2\right)^{-1.47} \tag{9}$$

with the prefactor again in units of MPa. As shown in Figure 1 (dashed lines), both empirical correlations result in good fits to the G_N^α data of the poly(α-olefins). The additional data point for poly(1-hexene) is taken from ref 1.

While these are empirical correlations, we argue that the backbone of the bottlebrush poly(α-olefin) is equivalent to diluted aPP, i.e., the side chains of the poly(α-olefin) polymers dilute their backbone chain. We assume that the effect of the side chains on the rheology is equivalent to that of a solvent consisting of low-molecular-weight oligomers, except that the oligomers are attached to the backbone. We recall that the plateau modulus of, e.g., PS dissolved in oligomers of the same chemistry decreases with the polymer fraction ϕ_m according to $\phi_m^{1+\alpha}$, see, e.g.[9,14,29] We take the dilution exponent α as equal to 1, while larger values of the dilution exponent (1 to 1.3) found experimentally can be attributed to the enhanced relaxation of chain ends as reported by Shahid et al.[30] We also note that Liu et al.[37] investigated the solvent effect of the short arm of entangled asymmetric PS star polymers. They demonstrated that the effect of the short arm on the plateau modulus is equivalent to the effect of short chains in binary blends consisting of linear long and short chains with equivalent weight fractions as in the asymmetric stars.

We therefore expect that the plateau modulus G_N^α of the poly(α-olefins) decreases with the virtual fraction ϕ_m of aPP contained in the poly(α-olefins) according to

$$G_N^\alpha = G_{PP} \phi_m^2 \tag{10}$$

G_{PP} is the plateau modulus of aPP. The ratio $\phi_m = m_{PP}/m_b = 3/(N_{sc} + 2)$ of the molecular weight $m_{PP} = 21$ g/mol per backbone bond of aPP to the respective molecular weight m_b of the α-olefins is given in Table 2. Equation 10 is shown in Figure 1 by the continuous red line and results in description of the G_N^α data based on reasonable assumptions without the need for any fit parameter. We can also

Table 2. Linear Viscoelastic Characterization of the Poly(α-olefin) Polymers at the Measurement Temperatures T

polymer	T [°C]	τ_R [s]	τ_d [s]	η_0 [Pa s]	ϕ_m [-]	ϕ [-]	$U/(3kT)$ [-]
aPP 25 °C	25	79.7	6.23×10^4	3.43×10^9	1	1	47
aPP 46 °C	46	2.21	1.89×10^3	1.02×10^8	1	1	44
PO	25	13.5	6.12×10^4	2.32×10^8	0.375	0.35	47
PD	7.6	24.8	5.32×10^4	1.83×10^8	0.300	0.29	50
PDD	3.3	31.7	1.92×10^5	1.36×10^8	0.250	0.25	51
PTD	60	0.56	7.57×10^2	1.52×10^6	0.214	0.22	42
POD	70	1.93	1.86×10^3	3.37×10^6	0.167	0.18	41

derive the fraction of aPP backbone contained in the poly(α-olefins) directly by the ratio of G_N^α to G_{PP},

$$\phi = \sqrt{G_N^\alpha/G_{PP}} \tag{11}$$

As seen from Table 2, there is excellent agreement of ϕ with ϕ_m, which confirms the assumption of backbone dilution. Thus, as far as the rheological behavior is concerned, we may consider the bottlebrush poly(α-olefins) as self-diluted aPP, i.e., as diluted aPP with the solvent molecules attached to the backbone. The effective fraction ϕ of the aPP backbone decreases with increasing side chain length from 1 for aPP to 0.35 for PO and to 0.18 for POD. The question may arise, why aPP is the correct reference for self-dilution of the poly(α-olefins) and why it is not polyethylene (PE). As also shown in Figure 1 (dotted red line), the relation $G_N^\alpha = G_{PE}(m_{PE}/m_b)^2$ with $G_{PE} = 2500$ kPa[13] and $m_{PE} = 14$ g/mol does not fit the plateau moduli of the poly(α-olefins). The steric effect of the methyl group in aPP reduces chain flexibility in comparison to PE as expressed by the decreased plateau modulus or the increased entanglement molecular weight of aPP. The same steric effect on the backbone flexibility is caused by the first methylene group (c1) of the alkane side chains of the poly(α-olefins), while the effect of c2 and higher, i.e., the effect of the number $N_{sc} - 1$ of side chain bonds on the plateau modulus can be expressed by eq10 with the aPP fraction $\phi_m = m_{PP}/m_b = 3/(3 + N_{sc} - 1)$.

Table 2 summaizes the linear viscoelastic characterization of the poly(α-olefin) polymers at the measurement temperature T.

3. ERS MODEL WITH DILUTION

The ERS model is a special form of the molecular stress function (MSF) model, which is a generalized tube segment model with strain-dependent tube diameter.[15−17] The extra stress tensor $\sigma(t)$ of the MSF model is given by a history integral of the form

$$\sigma(t) = \int_{-\infty}^t \frac{\partial G(t - t')}{\partial t'} f^2(t, t') \mathbf{S}_{DE}^{IA}(t, t') dt' \tag{12}$$

$G(t)$ is the relaxation modulus, t is the time of observation when the stress is measured, and t' indicates the time when a tube segment was created by reptation. The strain measure $\mathbf{S}_{DE}^{IA}$ represents the contribution to the extra stress tensor originating from the affine rotation of the tube segments according to the "Independent Alignment (IA)" assumption of Doi and Edwards[18,19] and is given by

$$\mathbf{S}_{DE}^{IA}(t, t') \equiv 5 \left\langle \frac{\mathbf{u}'\mathbf{u}'}{u'^2} \right\rangle_o = 5 \mathbf{S}(t, t') \tag{13}$$

with $\mathbf{S}(t, t')$ being the relative second-order orientation tensor. $\mathbf{u}'\mathbf{u}'$ is the dyad of a deformed unit vector $\mathbf{u}' = \mathbf{u}'(t, t')$,

$$\mathbf{u}' = \mathbf{F}_t^{-1} \cdot \mathbf{u} \tag{14}$$

$\mathbf{F}_t^{-1} = \mathbf{F}_t^{-1}(t, t')$ is the relative deformation gradient tensor, and u' is the length of $\mathbf{u}'$. The orientation average is indicated by $<...>_o$,

$$\langle ... \rangle_o \equiv \frac{1}{4\pi} \iint [...] \sin \theta_o d\theta_o d\varphi_o$$

i.e., an average over an isotropic distribution of unit vectors $\mathbf{u}$.

$f = f(t, t')$ represents the inverse of the relative tube diameter a/a_0, and at the same time, the relative length $l(t,t')$ of a deformed tube segment[10]

$$f(t, t') = \frac{a_0}{a(t, t')} = \frac{l(t, t')}{l_0} \tag{16}$$

At time $t = t'$, the tube segment was created with equilibrium tube diameter a_0 and equilibrium length l_0. Equation 16 is a direct consequence of equation (A9) of Doi and Edwards,[19] who showed that the line density n/l, i.e., the number n of Kuhn segments of length b that are found per length l of the tube, is a well-defined thermodynamic quantity and defines the tube diameter a by the relation $n/l = a/b^2$. For $f \equiv 1$, eq 12 reduces to the original Doi−Edwards IA model.

$\mathbf{S}_{DE}^{IA}$ is determined directly by the deformation history according to eq14, while the stretch f is found as solution of an evolution equation considering affine tube segment deformation balanced by enhanced Rouse relaxation.[10] With increasing stretch and decreasing tube diameter a, the number of monomers in a control volume of length and diameter a will decrease with the consequence of ERS in this control volume. The incremental increase of the relaxation rate with stretch is proportional to the fourth power of the stretch, and the relaxation rate therefore is proportional to the fifth power of the stretch. The evolution equation of the stretch $f(t,t')$ is obtained as a balance of extension rate versus relaxation rate

$$\frac{\partial f}{\partial t} = f(\mathbf{K}: \mathbf{S}) - \frac{f - 1}{\tau_R}(1 - \phi^4) - \frac{\phi^4(f^5 - 1)}{5\tau_R} \tag{17}$$

with initial condition $f(t, t' = 0) = 1$. The first term of the right-hand side of eq 17 expresses affine deformation with $\mathbf{K}$ being the deformation rate gradient, the second term Rouse stretch relaxation with Rouse time τ_R, and the third term takes into account ERS on smaller length scales. ϕ is the volume fraction of the polymer in solution. Note that for small stretches f with $f - 1 \ll 1$, eq17 reduces to the classical relation

$$\frac{\partial f}{\partial t} = f(\mathbf{K}: \mathbf{S}) - \frac{1}{\tau_R}(f - 1) \tag{18}$$

i.e., the evolution of stretch depends only on the deformation rate and the Rouse time. As shown by ref 10, the evolution eq17 can alternatively be expressed as a reduction of the monomeric friction coefficient ς by

$$\frac{\varsigma}{\varsigma_0} = \frac{5}{5(1 - \phi^4) + \phi^4(f^4 + f^3 + f^2 + f + 1)} \tag{19}$$

with ς_0 being the equilibrium friction coefficient. Thus, in this interpretation of the ERS model, friction decreases with increasing stretch, but the reduction of friction is delayed and reduced at lower polymer concentration.

According to the entropic fracture hypothesis,[20] brittle or elastic fracture will occur when the strain energy of a chain segment reaches the bond energy U of a carbon−carbon bond. Due to thermal fluctuations, the total strain energy of the chain segment will be concentrated on one C−C bond by thermal fluctuations, and the bond then ruptures. This leads to crack initiation and within a few milliseconds to macroscopic fracture. The critical stretch at fracture, f_c, is given by
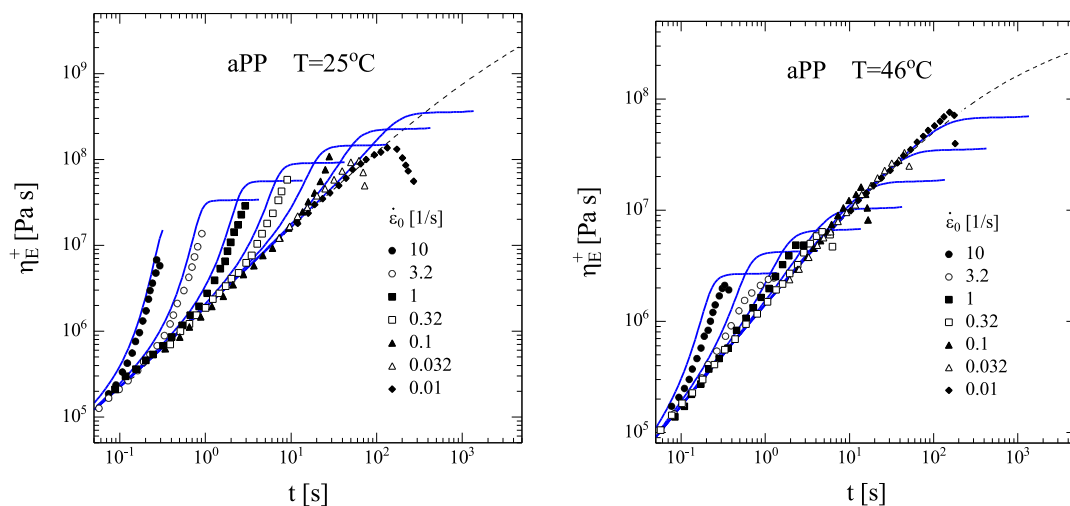
Figure 2. Comparison of the elongational stress growth coefficient $\eta_E^+(t)$ data (symbols) to the calculated results of the ERS model (lines) for aPP.

$$f_c = \sqrt{\frac{U}{3kT\phi}} \tag{20}$$

with k being the Boltzmann constant and T the absolute temperature. This fracture criterion has been shown to be in agreement with experimental evidence of polymer melts and solutions, see, e.g., refs 21−24.

4. COMPARISON OF ERS MODEL PREDICTIONS AND ELONGATIONAL VISCOSITY DATA OF POLY(α-OLEFIN) POLYMERS

Predictions of the ERS model with stress tensor eq12 and evolution of stretch eq17, and with the parameters τ_R and ϕ from Table 2, are compared in Figures 2 and 3 to the data (symbols) of the elongational stress growth coefficient $\eta_E^+(t)$ reported by López-Barrón and co-workers.[2] The atactic PP (Figure 2) at 25 and 46 °C shows the typical elongational behavior of a linear polymer with transient strain hardening starting at elongations rates $\dot{\varepsilon} \geq 1/\tau_R$ with τ_R calculated by eq5, followed by monotonous increasing transient strain-hardening with increasing strain rate. Calculated results (lines) of the ERS model are in line with this strain hardening behavior. The data of the elongational stress growth coefficient of aPP at 46 °C show some indication of transition to a steady-state elongational viscosity, in qualitative agreement with model predictions. At 25 °C and at small strain rates, $\eta_E^+(t)$ shows a maximum which is indicative of failure by inhomogeneous deformation, while at higher strain rate, sample fracture is observed before a steady state is reached. The maximal elongational viscosity reached experimentally is somewhat below the steady-state elongational viscosity predicted by the model, and according to the fracture criterion of eq 20, fracture would only be expected at the highest strain rate of $\dot{\varepsilon} = 10 \text{ s}^{-1}$ as indicated by the abrupt end of the predicted line before reaching the steady state.

For all the poly(α-olefin) bottlebrushes (Figure 3), the onset of strain hardening is in agreement with model predictions based on the Rouse times calculated by eq5. Also, the start-up of the elongational viscosity is well described by the ERS model for all elongation rates investigated. The samples were allowed to elongate in the Sentmanat extensional rheometer (SER) beyond the recommended maximum Hencky strain of $\varepsilon \leq 4$, above

which the sample starts to wind on itself. All the samples broke before reaching a Hencky strain of 4, except PTD (Figure 3d) and POD (Figure 3e) at strain rates above 1 s^{-1}. For PO (Figure 3a) and POD (Figure 3e), the maximal values of $\eta_E^+(t)$ are mostly in agreement with predictions, although the transition to a steady-state elongational viscosity is only seen at the lowest strain rates. Fracture according to the fracture criterion of eq20 is only expected at the highest strain rates and is indicated again by the abrupt end of the predicted lines. The samples of PD (Figure 3b) and PDD (Figure 3c) fractured already at much smaller strains than expected. We note that PD and PDD were measured at rather low temperatures, PD at only 7K above the melting temperature, and PDD above the glass transition temperature but below the melting temperature. While the ERS model gives a consistent description of the elongational stress growth of aPP and the poly(α-olefin) bottlebrushes, the cause of the premature fracture particularly of the samples of PD and PDD remains unclear.

Due to the different measurement temperatures and the different molecular weights, a direct comparison of the time-dependent elongational stress growth coefficients $\eta_E^+(t)$ and the strain hardening of the poly(α-olefin) bottlebrushes is not possible. However, from Figures 2 and 3 and except for PD and PDD, we may conclude the steady-state elongational viscosity predictions of the ERS model are in general agreement with the maximal elongational viscosity data measured and can therefore be used for a comparison of the elongational behavior of the poly(α-olefin) bottlebrushes. The normalized steady-state elongational viscosity η_E/η_0 or its maximal value in the case of fracture predicted by the ERS model is plotted in Figure 4a as a function of Weissenberg number $Wi_R = \dot{\varepsilon}\tau_R$. Lines are calculated by the ERS model and symbols indicate the calculated values at the experimental strain rates. Note that this is a temperature-invariant representation. aPP shows a monotonously decreasing elongational viscosity with a change of slope when strain hardening begins. The slope after the kink is approximately −0.4 as indicated by the red straight line. This is similar to the slope of log η_E as a function of log $\dot{\varepsilon}$ observed for other linear polymers, and it is higher than the slope of −1/2 expected from a one-mode ERS model. The higher slope is caused by the width of the relaxation spectrum, as already
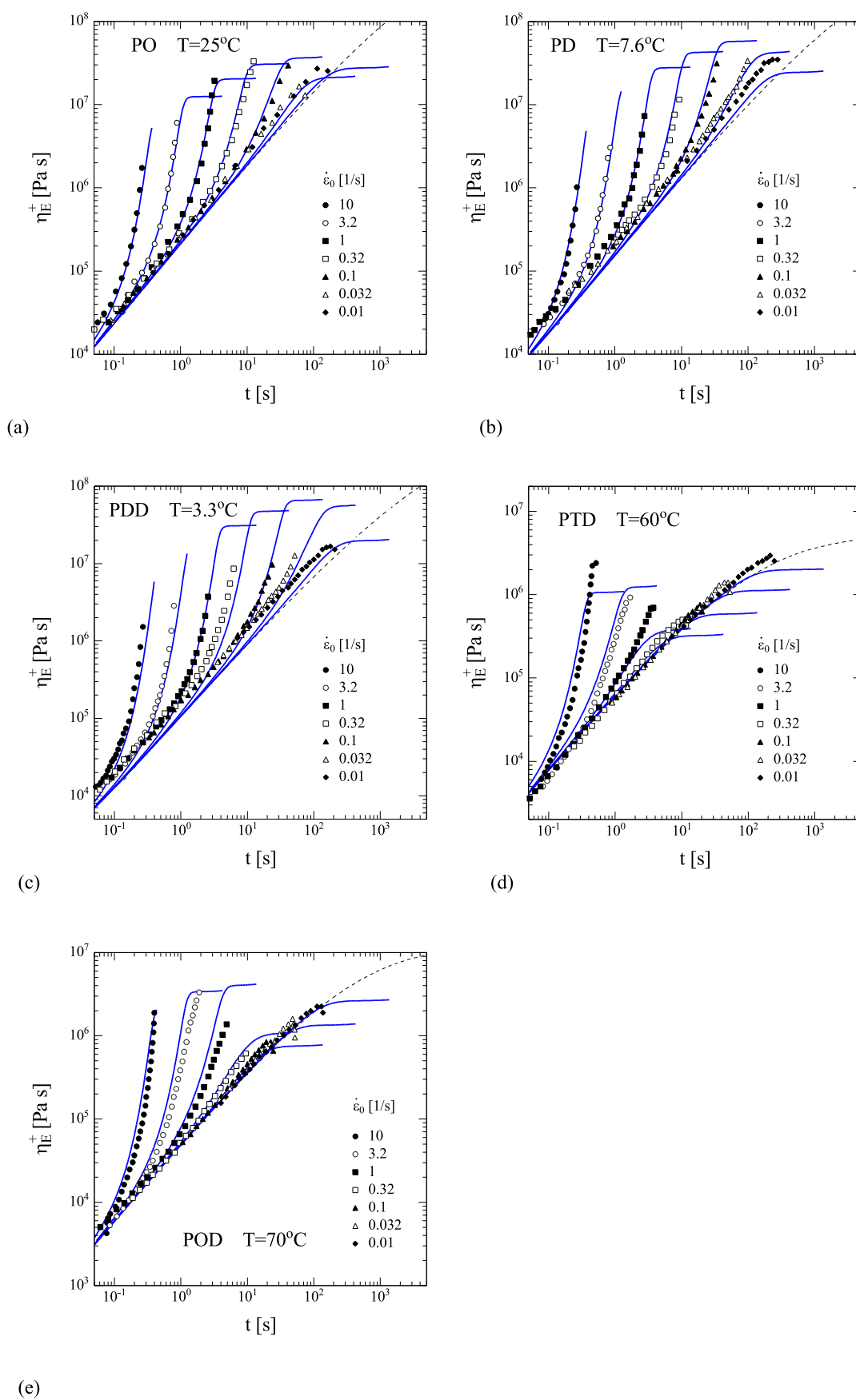
Figure 3. Comparison of the elongational stress growth coefficient $\eta_E^+(t)$ data (symbols) to the predictions of the ERS model (lines) for (a) poly(1-octene), (b) poly(1-decene), (c) poly(1-dodecene), (d) poly(1-tetradecene), and (e) poly(1-octadecene).
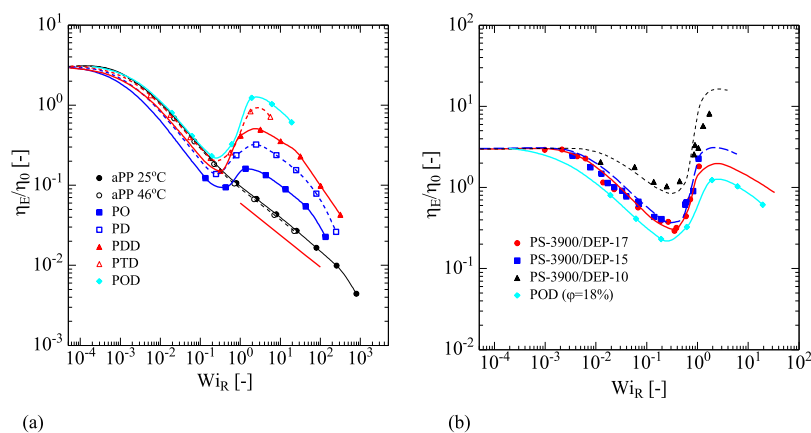
Figure 4. Normalized elongational viscosity η_E/η_0 as a function of Weissenberg number Wi_R for (a) of poly(α-olefin) bottlebrushes, and (b) for 17/15/10 weight% of PS3900 dissolved in DEP[26,27] and for POD. Straight red line in (a) indicates a slope of -0.4.

documented earlier for monodisperse PS melts.[25] For the poly(α-olefin) bottlebrushes, the elongational viscosity first decreases with increasing Wi_R, then increases and decreases again after a maximum in η_E. Figure 4a reveals a clear pattern of the strain hardening. The maximum in the elongational viscosity is the larger, the smaller the fraction of the backbone chain. The drop of η_E at high Wi_R is due to elastic fracture. We note that the elongational behavior of the poly(α-olefin) polymers is strikingly similar to that of entangled solutions of 3900 kg/mol polystyrene PS3900 in diethyl phthalate (DEP) investigated by Bhattacharjee and co-workers[26] and Acharya and co-workers.[27] This is shown in Figure 4b for solutions of PS3900/DEP with 17/15/10 weight% of PS and compared to POD with aPP backbone fraction of 18%. Due to the large difference between disengagement time τ_d and Rouse time τ_R, the elongational viscosity of the poly(α-olefin) bottlebrushes and the PS3900/DEP solutions is first reduced by increasing orientation, followed by strong strain-rate hardening when the Weissenberg number is approaching $Wi_R \cong 1$. Lines are predictions of the ERS model. Similar trends were also reported for other high molecular weight PS samples dissolved in oligomeric styrene.[14,28,29]

5. DISCUSSION AND CONCLUSIONS

The rheology of bottlebrush poly(α-olefin) polymers can be explained by considering that the alkane side chains with 6−16 carbons dilute the backbone chain. As far as the rheology is concerned, poly(α-olefin) can be considered as diluted aPP with the solvent molecules consisting of alkane oligomers attached to the backbone. The plateau modulus of the poly(α-olefins) decreases with increasing length of the side chain according to $G_\alpha^0 = G_{aPP}^0 \phi^2$, and the diluted fraction ϕ of the backbone derived from this relation agrees with the ratio of molecular weight per backbone bond of aPP to that of the poly(α-olefins). The Rouse time τ_R as obtained from Osaki's relation[12] is in good concord with the onset of transient strain hardening observed experimentally at elongation rates $\dot{\varepsilon} \geq 1/\tau_R$, if we consider that the effective τ_R in the case of the polydisperse melts is determined by the longer molecules. Overall, the ERS model and the fracture criterion of eq 20 provide a consistent description of the elongational rheology of the bottlebrush poly(α-olefins), even with the early fracture especially of the PD and PDD samples remaining unexplained.

López-Barrón and co-workers[2] attributed the strain hardening of bottlebrush poly(α-olefins) to an increase in side chain interdigitation as soon as the polymers align in the flow direction. They postulated an increase in intermolecular friction by side chain interaction. Based on friction reduction interpretation of the ERS model according to eq 19, we can now test the validity of this conjecture. Figure 5 presents the
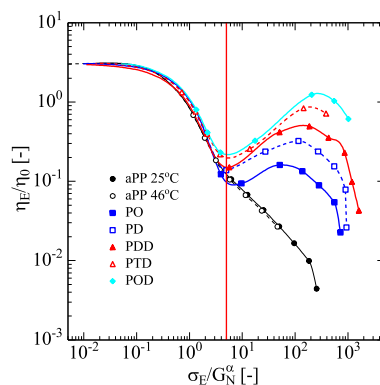

Figure 5. Normalized elongational viscosity $\eta_E(\sigma_E)/\eta_0$ as a function of elongational stress σ_E normalized by the plateau modulus G_N^α. Vertical red line indicates $\sigma_E = 5 G_N^\alpha$.

normalized elongational viscosity η_E/η_0 as a function of the tensile stress $\sigma_E = \eta_E \dot{\varepsilon}$, and the tensile stress is normalized by the plateau modulus G_N^α. All the curves coincide initially until reaching the vertical red line at $\sigma_E = 5 G_N^\alpha$, which signifies full orientation according to the Doi−Edwards IA model. We conclude that the first part of the conjecture is confirmed. Strain hardening starts after full orientation of the polymer chains, and the distinct separation of orientation and stretch is due to the large difference between disengagement time τ_d and Rouse time τ_R of the polymers considered. However, concerning the strain hardening part of the conjecture in terms of intermolecular friction, instead of an increase of friction by interdigitation, strain hardening is rather caused by delayed and reduced friction reduction with a decreasing fraction of the diluted aPP backbone as seen from eq 19. Alternatively, in the tube model interpretation of the ERS model, the tube diameter at equilibrium increases from the tube diameter a_0^{aPP} of aPP to

the tube diameter $a_0^\alpha = a_0^{aPP}\phi^{-1/2}$ of the poly(α-olefins) due to self-dilution in agreement with their smaller plateau modulus. A larger tube diameter allows for a larger stretch. This is reflected in the relaxation term of the stretch evolution eq17 by the factor ϕ^4, which leads to high strain rates to a steady-state stretch f_{ss} of ref 10

$$f_{ss} = \phi^{-1}\sqrt[4]{5\dot{\varepsilon}\tau_R} = \phi^{-1}\sqrt[4]{5Wi_R} \tag{21}$$

The limiting stretch f_{ss} increases with increasing dilution and decreasing polymer fraction; i.e., more diluted polymer solutions show more strain hardening than less diluted ones, see, e.g., refs 9,28,29. This results in a limiting elongational stress of

$$\sigma_E = 5G_N^\alpha f_{ss}^2 = 5\sqrt{5}\,G_N^\alpha \phi^{-2}\sqrt{Wi_R} = 5\sqrt{5}\,G_N^{aPP}\sqrt{Wi_R} \tag{22}$$

The universal relation 22 is shown in Figure 6 by the straight red line with a slope of 1/2. All the poly(α-olefins) reach the
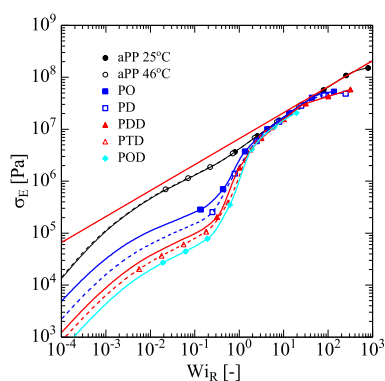

Figure 6. Elongational stress σ_E as a function of the Weissenberg number $Wi_R = \dot{\varepsilon}\tau_R$. Straight line with slope 1/2 is given by $\sigma_E = 5\sqrt{5}\,G_N^{aPP}\sqrt{Wi_R}$.

same elongational stress as given by eq22 at high Wi_R. At even higher Wi_R, the stress is expected to level off due to sample fracture. We can also see from Figure 6 that significant strain hardening starts already at Weissenberg numbers above $Wi_R \cong 0.3$.

In conclusion, the specific elongational rheology of poly(α-olefin) bottlebrushes with entangled backbone and unentangled side chains can be explained by self-dilution of the backbone by the side chains and can be described by the ERS model. This is expected to be true for other bottlebrush polymer systems with entangled backbones as well, as long as the side chains are not entangled, such as the model poly(n-alkyl methacrylate)s investigated by Wu et al.[36] Based on the data of Abbasi et al.,[7] Hirschberg et al.[34] have shown that from bottlebrushes to loosely grafted combs, the diluted plateau modulus of the backbone decreases with the square of the backbone fraction ϕ_{bb}. Therefore, we expect that our modeling will still be valid if the graft density decreases from bottlebrushes to loosely crafted combs to linear aPP (as shown here in Figure 2), as long as the side chains are not entangled. However, a qualitative change of the elongational behavior occurs,[7,35] if the length of the side chains approaches the entanglement limit, and/or the backbone after dilution will no longer be entangled.

■ **AUTHOR INFORMATION**

Corresponding Authors

   Manfred H. Wagner − *Polymer Engineering/Polymer Physics, Berlin Institute of Technology (TU Berlin), 10587 Berlin, Germany;* ● orcid.org/0000-0002-1815-7060; Email: manfred.wagner@tu-berlin.de

   Valerian Hirschberg − *Institute of Chemical Technology and Polymer Chemistry (ITCP), Karlsruhe Institute of Technology (KIT), 76131 Karlsruhe, Germany;* ● orcid.org/0000-0001-8752-930X; Email: valerian.hirschberg@kit.edu

Complete contact information is available at:
https://pubs.acs.org/10.1021/acs.macromol.3c02430

Notes

The authors declare no competing financial interest.

■ **REFERENCES**

(1) López-Barrón, C. R.; Tsou, A. H.; Hagadorn, J. R.; Throckmorton, J. A. Highly Entangled α-Olefin Molecular Bottlebrushes: Melt Structure, Linear Rheology, and Interchain Friction Mechanism. *Macromolecules* **2018**, *51* (17), 6958−6966.

(2) López-Barrón, C. R.; Shivokhin, M. E.; Hagadorn, J. R. Extensional rheology of highly-entangled α-olefin molecular bottlebrushes. *J. Rheol.* **2019**, *63* (6), 917−926.

(3) López-Barrón, C. R.; Shivokhin, M. E. Extensional Strain Hardening in Highly Entangled Molecular Bottlebrushes. *Physical review letters* **2019**, *122* (3), 37801.

(4) Abbasi, M.; Faust, L.; Wilhelm, M. Comb and Bottlebrush Polymers with Superior Rheological and Mechanical Properties. *Advanced materials (Deerfield Beach, Fla.)* **2019**, *31* (26), No. e1806484.

(5) Dealy, J. M. *Structure and Rheology of Molten Polymers: From Polymerization to Processability:From structure to flow behavior and back again*; Hanser Gardner Publications, 2006.

(6) McLeish, T. C. B.; Larson, R. G. Molecular constitutive equations for a class of branched polymers: The pom-pom polymer. *J. Rheol.* **1998**, *42* (1), 81−110.

(7) Abbasi, M.; Faust, L.; Riazi, K.; Wilhelm, M. Linear and Extensional Rheology of Model Branched Polystyrenes: From Loosely Grafted Combs to Bottlebrushes. *Macromolecules* **2017**, *50* (15), 5964−5977.

(8) Matsumiya, Y.; Watanabe, H. Non-Universal Features in Uniaxially Extensional Rheology of Linear Polymer Melts and Concentrated Solutions: A Review. *Prog. Polym. Sci.* **2021**, *112*, No. 101325.

(9) Narimissa, E.; Huang, Q.; Wagner, M. H. Elongational rheology of polystyrene melts and solutions: Concentration dependence of the interchain tube pressure effect. *J. Rheol.* **2020**, *64* (1), 95−110.

(10) Wagner, M. H.; Narimissa, E. A new perspective on monomeric friction reduction in fast elongational flows of polystyrene melts and solutions. *J. Rheol.* **2021**, *65* (6), 1413−1421.

(11) Wagner, M. H.; Narimissa, E.; Masubuchi, Y. Elongational viscosity of poly(propylene carbonate) melts: tube-based modelling and primitive chain network simulations. *Rheol. Acta* **2023**, *62* (1), 1−14.

(12) Osaki, K.; Nishizawa, K.; Kurata, M. Material time constant characterizing the nonlinear viscoelasticity of entangled polymeric systems. *Macromolecules* **1982**, *15* (4), 1068−1071.

(13) Fetters, L. J.; Lohse, D. J.; García-Franco, C. A.; Brant, P.; Richter, D. Prediction of Melt State Poly(α-olefin) Rheological Properties: The Unsuspected Role of the Average Molecular Weight per Backbone Bond. *Macromolecules* **2002**, *35* (27), 10096−10101.

(14) Huang, Q.; Hengeller, L.; Alvarez, N. J.; Hassager, O. Bridging the Gap between Polymer Melts and Solutions in Extensional Rheology. *Macromolecules* **2015**, *48* (12), 4158−4163.

(15) Narimissa, E.; Wagner, M. H. Review of the hierarchical multi-mode molecular stress function model for broadly distributed linear and LCB polymer melts. *Polym. Eng. Sci.* **2019**, *59* (3), 573−583.

(16) Narimissa, E.; Wagner, M. H. Review on tube model based constitutive equations for polydisperse linear and long-chain branched polymer melts. *J. Rheol.* **2019**, *63* (2), 361−375.

(17) Wagner, M. H.; Rubio, P.; Bastian, H. The molecular stress function model for polydisperse polymer melts with dissipative convective constraint release. *J. Rheol.* **2001**, *45* (6), 1387−1412.

(18) Doi, M.; Edwards, S. F. Dynamics of concentrated polymer systems. Part 4.—Rheological properties. *J. Chem. Soc., Faraday Trans. 2* **1979**, *75* (0), 38−54.

(19) Doi, M.; Edwards, S. F. Dynamics of concentrated polymer systems. Part 3.—The constitutive equation. *J. Chem. Soc., Faraday Trans. 2* **1978**, *74* (0), 1818−1832.

(20) Wagner, M. H.; Narimissa, E.; Huang, Q. Scaling relations for brittle fracture of entangled polystyrene melts and solutions in elongational flow. *J. Rheol.* **2021**, *65* (3), 311−324.

(21) Wagner, M. H.; Narimissa, E.; Poh, L.; Shahid, T. Modeling elongational viscosity and brittle fracture of polystyrene solutions. *Rheol. Acta* **2021**, *60* (8), 385−396.

(22) Wagner, M. H.; Hirschberg, V. Experimental validation of the hierarchical multi-mode molecular stress function model in elongational flow of long-chain branched polymer melts. *J. Non-Newtonian Fluid Mech.* **2023**, *321*, No. 105130.

(23) Wagner, M. H.; Narimissa, E.; Poh, L.; Huang, Q. Modelling elongational viscosity overshoot and brittle fracture of low-density polyethylene melts. *Rheol. Acta* **2022**, *61* (4−5), 281−298.

(24) Wagner, M. H.; Narimissa, E.; Shahid, T. Elongational viscosity and brittle fracture of bidisperse blends of a high and several low molar mass polystyrenes. *Rheol. Acta* **2021**, *60* (12), 803−817.

(25) Wagner, M. H.; Kheirandish, S.; Koyama, K.; Nishioka, A.; Minegishi, A.; Takahashi, T. Modeling strain hardening of polydisperse polystyrene melts by molecular stress function theory. *Rheol. Acta* **2005**, *44* (3), 235−243.

(26) Bhattacharjee, P. K.; Oberhauser, J. P.; McKinley, G. H.; Leal, L. G.; Sridhar, T. Extensional Rheometry of Entangled Solutions. *Macromolecules* **2002**, *35* (27), 10131−10148.

(27) Acharya, M. V.; Bhattacharjee, P. K.; Nguyen, D. A.; Sridhar, T.; Co, A.; Leal, G. L.; Colby, R. H.; Giacomin, A. J. Are Entangled Polymeric Solutions Different from Melts? In *AIP Conference Proceedings*; AIP, 2008; 391−393.

(28) Shahid, T.; Clasen, C.; Oosterlinck, F.; van Ruymbeke, E. Diluting Entangled Polymers Affects Transient Hardening but Not Their Steady Elongational Viscosity. *Macromolecules* **2019**, *52* (6), 2521−2530.

(29) André, A.; Shahid, T.; Oosterlinck, F.; Clasen, C.; van Ruymbeke, E. Investigating the Transition between Polymer Melts and Solutions in Nonlinear Elongational Flow. *Macromolecules* **2021**, *54* (6), 2797−2810.

(30) Shahid, T.; Huang, Q.; Oosterlinck, F.; Clasen, C.; van Ruymbeke, E. Dynamic dilution exponent in monodisperse entangled polymer solutions. *Soft Matter* **2017**, *13*, 269−282.

(31) Ianniruberto, G.; Brasiello, A.; Marrucci, G. Friction Coefficient Does Not Stay Constant in Nonlinear Viscoelasticity. In *7th Annual European Rheology Conference*; Suzdal, Russia, 2011; 61.

(32) Ianniruberto, G.; Marrucci, G.; Masubuchi, Y. Melts of Linear Polymers in Fast Flows. *Macromolecules* **2020**, *53*, 5023−5033.

(33) Huang, Q. When Polymer Chains Are Highly Aligned: A Perspective on Extensional Rheology. *Macromolecules* **2022**, *55* (3), 715−727.

(34) Hirschberg, V.; Schußmann, M. G.; Ropert, M. C.; Wilhelm, M.; Wagner, M. H. Modeling elongational viscosity and brittle fracture of by the hierarchical molecular stress function model. *Rheol. Acta* **2023**, *62*, 269−283.

(35) Hirschberg, V.; Faust, L.; Abbasi, M.; Huang, Q.; Wilhelm, M.; Wagner, M. H. Hyperstretching in Elongational Flow of Densely Grafted Comb and Branch-on-Branch Model Polystyrenes. *J. Rheol.* **2024**. Accepted

(36) Wu, S.; Yang, H.; Chen, Q. Nonlinear Extensional Rheology of Poly(n-alkyl methacrylate) Melts with a Fixed Number of Kuhn Segments and Entanglements per Chain. *ACS Macro Lett.* **2022**, *11* (4), 484−490.

(37) Liu, S.; Zhang, J.; Hutchings, L. R.; Peng, L.; Huang, X.; Huang, Q. The "solvent" effect of short arms on linear and nonlinear shear rheology of entangled asymmetric star polymers. *Polymer* **2023**, *281*, No. 126125.